Steel and Composite Structures, Vol. 14, No. 4 (2013) 313-333
DOI: http://dx.doi.org/10.12989/scs.2013.14.4.313

Experimental and theoretical research on mechanical behavior of innovative composite beams

Gang Zhu[1,2], Yong Yang[1], Jianyang Xue[*1] and Jianguo Nie[3]

[1]*College of Civil Engineering, Xi'an University of Arch. and Tech., Shaan Xi, Xi'an, 710055, P.R. China*
[2]*China Haisum Engineering Co. Ltd., Shanghai, 200031, P.R. China*
[3]*Department of Civil Engineering, Tsinghua University, Beijing, 100084, P.R. China*

(Received October 12, 2010, Revised December 10, 2012, Accepted February 14, 2013)

Abstract. The web-encased steel-concrete composite (WESCC) beam is a new developed steel-concrete composite beam. Experiments of six simply supported WESCC beam specimens were conducted. The effects of the shear-span ratio and steel section type were all investigated on the static behaviors such as failure modes, failure mechanism and bearing capacity. The experimental results denoted that all specimens failed in bending mode and the degree of combination between the bottom armor plate of steel shape and concrete were very well without any evident slippage, which demonstrated that the function of bottom armor plate and web were fully exerted in the WESCC beams. It could be concluded the WESCC beams have high stiffness, high load carrying capacity and advanced ductility. The design methods are proposed which mainly consist the bearing capacity calculation of bending and flexural rigidity. The calculation results of the bearing capacity and deflection which take the shear deflection into account are in agreement with the experimental results. The design methods are useful for design and application of the innovative composite beams.

Keywords: composite beams; experiment study; mechanical behavior; bearing capacity; flexural rigidity; shear deflection

1. Introduction

The web-encased steel-concrete composite (WESCC) beam is a new type of steel-concrete composite beam which develops on the basis of the investigation and application of steel-concrete composite beam (many researchers have carried out investigations on it, Amadio 2004, Jurkiewiez 2007, Nie 2009, Zhang 2009, Valente 2010, Pecce 2012, Won 2012) and steel reinforced concrete beam (Lu 2006, Benitez1998, Ju 2001, Ju 2009). Perfobond ribs (which usually be abbreviated as PBL) connectors (Oguejiofor 1997, Nishiumi 1999, Medberry 2002, Cândido 2010) were used in WESCC beam to replace traditional stud connectors and transfer shear force occurred in the place between rib of girder and top concrete flange, which provides the WESCC beam effective connection without specialized stud welding equipment. Its main constitution way is that the stirrup are penetrated into the web of steel girder and then poured concrete with top flange plate simultaneously which forms web-encased steel-concrete composite beam with cast-in-place

*Corresponding author, Professor, E-mail: jianyang_xue@163.com

reinforced concrete top flange plate. The bottom flange plate of steel girder of WESCC beam is in state of exposure. The speed development of crack of WESCC beam with the concrete confined by steel flange is lower than that of the steel composite beam in normal loading range. The web of steel girder is enwrapped and confined by concrete which is similar to steel reinforced concrete beam (Johnson 1982, Narayanan 1988). So the WESCC beam needn't take stability of the steel girder into account and the bearing capacity of WESCC beam is higher than that of steel-concrete composite beam. Therefore, a series of experimental research have been carried out to research the mechanical behaviors and design methods of the new type of beam. On the basis of experimental investigation, the flexural experimental studies of WESCC beams were conducted so as to establish the calculation methods of cross-section flexural bearing capacity and flexural stiffness.

2. Experimental investigation

2.1 Specimen design

In order to study the mechanical properties and failure modes of specimens, six simply supported composite beams were designed and constructed. The main experimental parameters were shear span ratio and steel form of WESCC beam. Figs. 1-3 show the main details of the specimens. Specimens were divided into three types in team of different inner steel form. Steel form of type I: the steel I-beam in WESCC beam shows in Fig. 2(a). Steel form of type II: the steel I-beam without top flange in WESCC beam shows in Fig. 2(b). Steel form of type III: the steel I-beam with the corrugated steel web and without top flange shows in Fig. 2(c). Table 1 shows the testing matrix.

(a) Steel form of Type II

(b) Steel form of Type III

Fig. 1 Constructional detail of specimens

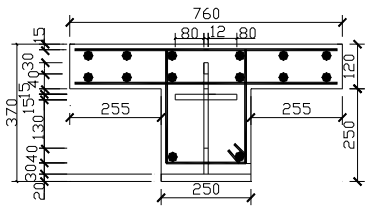

(a) Steel form of type I

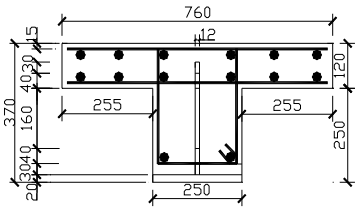

(b) Steel form of type II

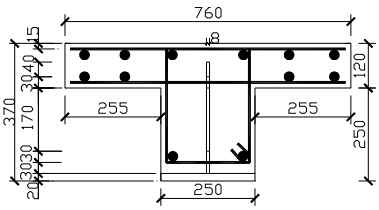

(c) Steel form of type III

Fig. 2 Schematic diagram of section of the composite beams

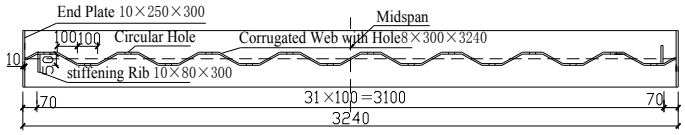

(a) Inner steel form of specimen CB-3-740

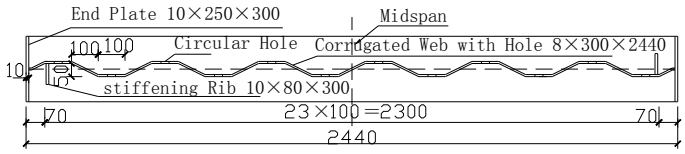

(b) Inner steel form of specimen CB-3-1740

Fig. 3 Steel form of type III with corrugated steel web

Table 1 Testing matrix

Specimen	L_0 (mm)	a (mm)	L_p (mm)	λ (mm)	T_{ro}	T_{lo}	Steel form	Steel ratio
CB-1-740	2340	340	860	2.0	0.26%	1.2%	I	6.5%
B-1-1740	3140	740	860	3.1	0.26%	1.2%		6.5%
CB-2-740	2340	1140	860	2.0	0.26%	1.2%	II	5.0%
B-2-1740	3140	340	860	3.1	0.26%	1.2%		5.0%
CB-3-740	2340	740	860	2.0	0.26%	1.2%	III	4.5%
B-3-1740	3140	1740	860	3.1	0.26%	1.2%		4.5%

Note: L_0 = calculation span length; λ = shear span ratio, λ = a/h, a and h = shear span and height of the composite beam; L_p = pure bending span length; T_{ro} = volume ratio of transverse reinforcement; T_{lo} = volume ratio of longitudinal reinforcement

The main materials of specimens are steel Q235, reinforcement HRP335, HPB235, where, the longitudinal reinforcements are 14, the lateral distributive reinforcements in concrete flange are HRP335, 10@250, and Stirrups are HPB235, 10@200. Together with each specimen, concrete cubes and prisms (a common practice in China) were cast to test the axial compressive strength. These cubes were cured and kept under the same conditions as the test specimens. The concrete strength was determined based on compression tests of concrete cubes according to the Chinese standards. The concrete test blocks were tested by the computerized automatic concrete cube crushing machine. The properties of steel and concrete are summarized in Table 2.

2.2 Load and measurement program

The experiment has been done in the Structure and Seismic Laboratory of Huaqiao University. Static loading tests were conducted on six WESCC beams. All specimens in the experiment were simply supported with two symmetrical concentrated loading way. Two 300 kN hydraulic jacks were placed at each loading point which were connected by one oil pipe so as to apply equal monotonic load. Two hydraulic jacks were both accurately calibrated. Reaction frame was installed at the loading place and the bottom of which was fixed in geosynclines. The distribution beams under the jack were used to transfer load to the top concrete flange. In order to transfer the load

evenly, half spherical hinge was fixed at the place which is between jack and distribution beam. The steel plate was set at the bottom supporting point under composite beam so as to prevent local deformation of the bottom steel plate. Building structural adhesive was deposited not only between steel plate and composite beam but also between distribution beam and top of the beam so as to make the interface smooth.

Vertical load and development of cracks are recorded during the loading period. Strain distribution over the depth of the steel section at the main loading stages and the midspan moment-deflection curve of test beams were all analyzed. All the experimental data was collected automatically and continuously by DH3816 static strain measurement system with one-second interval. Arrangement diagram of measuring point is shown in Fig. 4.

Table 2 Summary of material properties

Specimen	Steel material properties					Concrete material properties		
	E_s ($\times 10^5$ N/mm^2)	Strength of steel (N/mm^2)				E_c ($\times 10^4$ N/mm^2)	Strength of concrete (N/mm^2)	
		f_y		f_u			f_{cu}	f_c
		Web	Flange	Web	Flange			
CB-1-740	2.06	300	305	450	460	2.58	57.67	42.24
CB-1-1740	2.06					2.58	57.67	42.24
CB-2-740	2.06					3.08	57.96	43.33
CB-2-1740	2.06					2.93	59.67	43.71
CB-3-740	2.06					2.80	49.58	37.68
CB-3-1740	2.06					2.80	49.58	37.68

Note: E_s = elastic modulus of steel; E_c = elastic modulus of concrete; f_c = the axial compressive strength of concrete; f_{cu} = the cubic strength of concrete

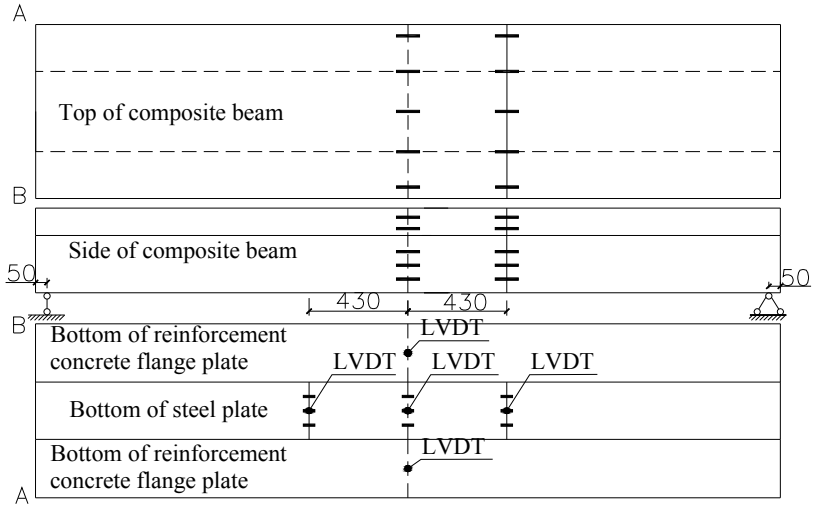

Fig. 4 Layout of strain gauges and LVDT

3. Experimental results and discussion

3.1 Test process and failure behavior

The monotonic static load was provided by 300 t separation hydraulic jacks with 2 kN increment each level so as to observe the development of cracks, deflection and failure modes of the specimens.

The failure mode of six specimens is all bending failure. The damage of the beams wasn't caused by the failure of the connectors. At the initial load stage, about 10% P_u ~ 20% P_u (P_u is ultimate load), the first tiny crack appeared at the central part of the side concrete surface of pure bending segment of the specimens. When the load was at 30% P_u ~ 40% P_u, the concrete cracking sound can be heard intermittently from the loading point, which indicates that the chemical bonding between the bottom steel plate of the beam and concrete began to undermine when cracks appeared. With the increment of the load, the concrete cracking sound became more evident. The cracks at the place between the bottom steel plate of the beam and concrete got further development. Therefore, the longitudinal shear force was provided by the end seal plate of beam and the stirrups penetrated into the web of steel girder. At this time, the first batch of cracks at the side concrete surface of pure bending segment developed sufficiently. The average width of the cracks was only 0.05 mm, crack spacing was about 400 mm. While the load was increasing continuously, the crack developed slowly which indicated the good restriction of bottom steel plate to concrete. When the load reached 50% P_u ~60% P_u, diagonal shear crack appeared at the position near the support of the beam and about 70mm distance away from the bottom of the beam. The crack developed along the diagonal direction to the loading point and the support of the beam with

(a) Cracks of the pure bending segment

(b) Cracks of the flexure shear segment

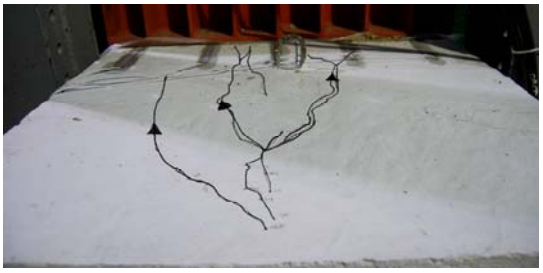

(c) Longitudinal cracks of deck

Fig. 5 Typical crack model of composite beam

Fig. 6 Flexure failure (Shear span ratio = 3.1)

Fig. 7 Flexure failure (Shear span ratio = 2.0)

width about 0.1 mm. The second batch of cracks appeared between the first batch of cracks with spacing of approximately 200 mm. At this time, the cracks at bending and shear segment developed very slowly. When the load arrived at 70% P_u~80% P_u, the bending cracks at the side concrete surface between mid-span and loading point developed to the underside of the reinforced concrete flange. The horizontal and vertical cracks appeared at the underside of the reinforced concrete flange which extended to side of the reinforced concrete flange with spacing of 200 mm. Then two cracks appeared on the surface of the reinforced concrete flange which developed from loading point to end of the reinforced concrete flange, as shown in Fig. 5.

When the load was at the ultimate load P_u, the crack width of the composite beam with shear span ratio 3.1 reached 3.5 mm, and the crack width at shear span just reached 1.0 mm. As to the beam with a shear span ratio of 2.0, the cracks width at shear span reached 1.2 mm, but the cracks width at the pure bending segment reached 3.5 mm. At final stage of the test, the top reinforced concrete flange at mid-span crushed and bulged, and the internal reinforcements revealed at the same time. The deflection of mid-span and the loading point developed very fast while the load declined quickly. At this time, the specimen of WESCC beam damaged and the load stopped. The typical failure modes are shown in Figs. 6 and 7.

3.2 Strain distribution over the depth of the WEBCC beam

Fig. 8 shows the strain distribution over the depth of the specimens CB-1-1140, CB-1-740. Where y is the height along cross-section of the beam, $y = 0$ is the bottom of the beam, $y = 370$ is the top of the beam, P_u is the measured ultimate load carrying capacity, P/P_u is the measured load ratio. As it can be seen from Fig. 8, the recorded strain results indicated that longitudinal strain along the cross-section was near linear distribution and the strain distribution of the section conformed to the plane cross-section assumption.

3.3 Strain development of the bottom steel plate and web

As shown in Fig. 9, strain of the bottom steel plate has already passed the yield strain when the beam reached the maximum bearing capacity, the yield strain $\varepsilon_y = f_y / E_s$ =1480 $\mu\varepsilon$. The maximum strain of the bottom steel plate of steel form of type I and II reached 9000~10000 $\mu\varepsilon$ and steel form of type III with corrugated steel web reached 5000~6000 $\mu\varepsilon$. The strain development of the bottom

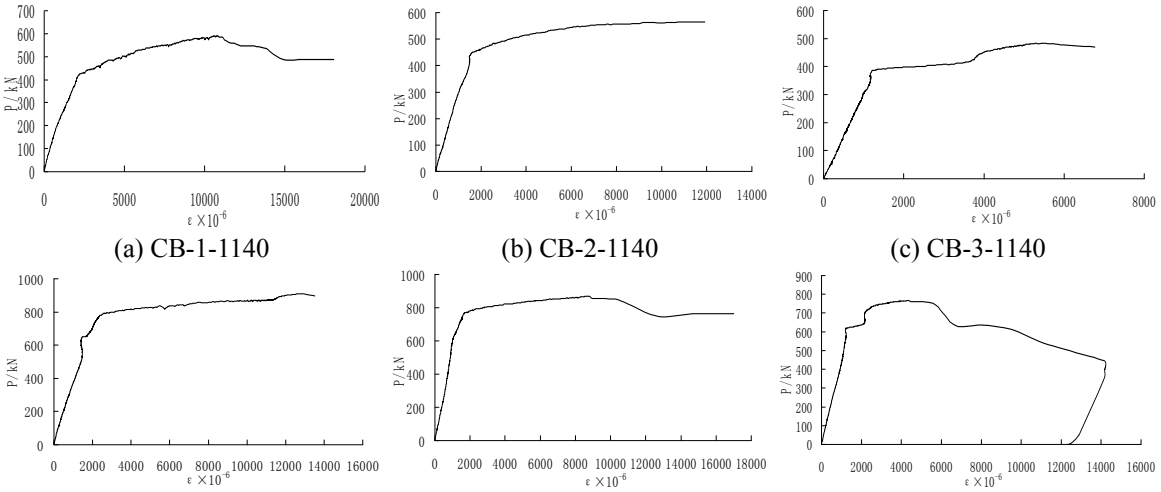

(a) CB-1-1140 (b) CB-2-1140 (c) CB-3-1140

(d) CB-1-740 (e) CB-2-740 (f) CB-3-740

Fig. 9 Curve of load vs. strain of bottom armor plate at midspan of specimens

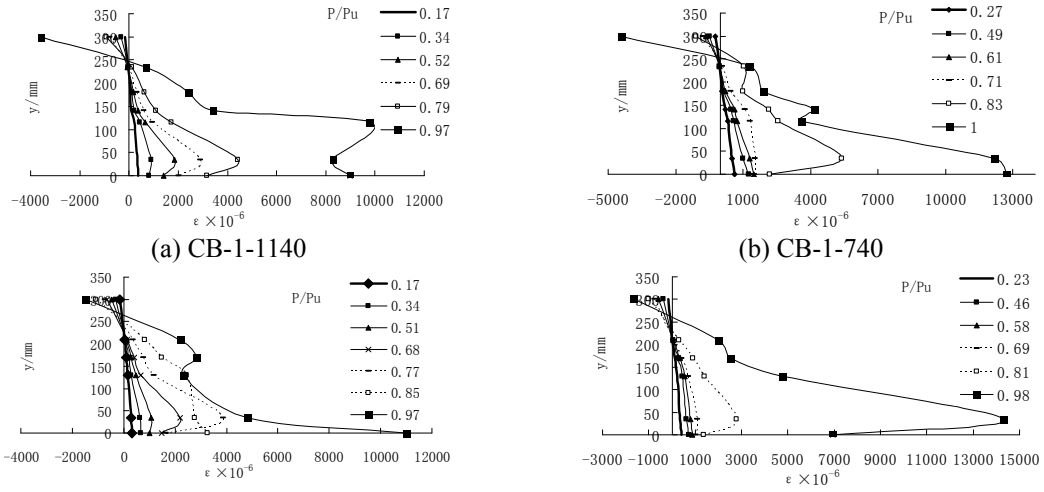

(a) CB-1-1140 (b) CB-1-740

(c) CB-2-1140 (d) CB-2-740

Fig. 10 Strain distribution over the depth of the steel section at main load segments

steel plate developed slowly before the bottom steel plate yielded, but quickly if the bottom steel plate has yielded, and then the composite beam failured with advanced ductility. Strain distribution of steel section is shown in Fig. 10. $y = 0$ is the place at the underside of the steel, $y = 320$ is the place at the top of shear connectors. When the beam reached the ultimate load, steel yielded and entered the strengthening phase. The plastic section formed. The tension strain of web near the hole was large, and the web round the hole was mainly weakened by stress concentration. Plastic neutral of cross-section is at the junction of PBL and steel web, which indicated that the steel of type II, III in WESCC beam was mostly in the tension region and fully utilized. For the steel form of type I, plastic neutral of the cross-section was nearby the top steel flange which had no evident function for changing mechanical properties of the beam.

3.4 Midspan moment-deflection curve

Midspan moment-deflection curves of test beams are shown in Fig. 11, experimental results show that the midspan moment-deflection curves of WESCC beam is similar to those of the steel-concrete composite beam. The WESCC beam went through elastic stage, elastic-plastic stage and load degenerating stage during the whole test procedure.

Considering the main contribution of the bottom steel plate to the flexural capacity, this article defines the moment corresponded to the yielding of the bottom steel plate as yield moment M_y of specimen. Therefore, M_y is as demarcation point of elastic stage and elastic-plastic stage. At elastic stage, midspan moment-deflection curve essentially took on linear variation. At the state between yielding of bottom steel plate and crushed of top concrete, the stiffness of specimens gradually decreased due to the development of cracks at midspan and shear span. The tempo of deflection was much greater than that of loading. Midspan moment-deflection took on non-linear variation. Owing to a majority of load undertook by bottom steel plate, the integral rigidity of composite beam hadn't evident degradation. But it declined quickly after reaching ultimate load. Midspan moment-deflection curve had a smooth descending stage and brittle failure of composite beam didn't occur. The WESCC beam had good ductility and deformation ability throughout the whole test procedure.

3.5 Analysis of bending performance of WESCC beam

The main test results are summarized in Table 3, the moment corresponded to the yielding of the bottom steel plate is defined as yield moment M_y, V_y and M_y are recorded values of shear and moment when the specimens started to yield. V_u and M_u are the biggest recorded values of shear force and moment of specimens. δ_y and δ_u are recorded deflection corresponding to M_y and M_u.

As to WESCC beams, three types of beams with different inner steel form have similar yield

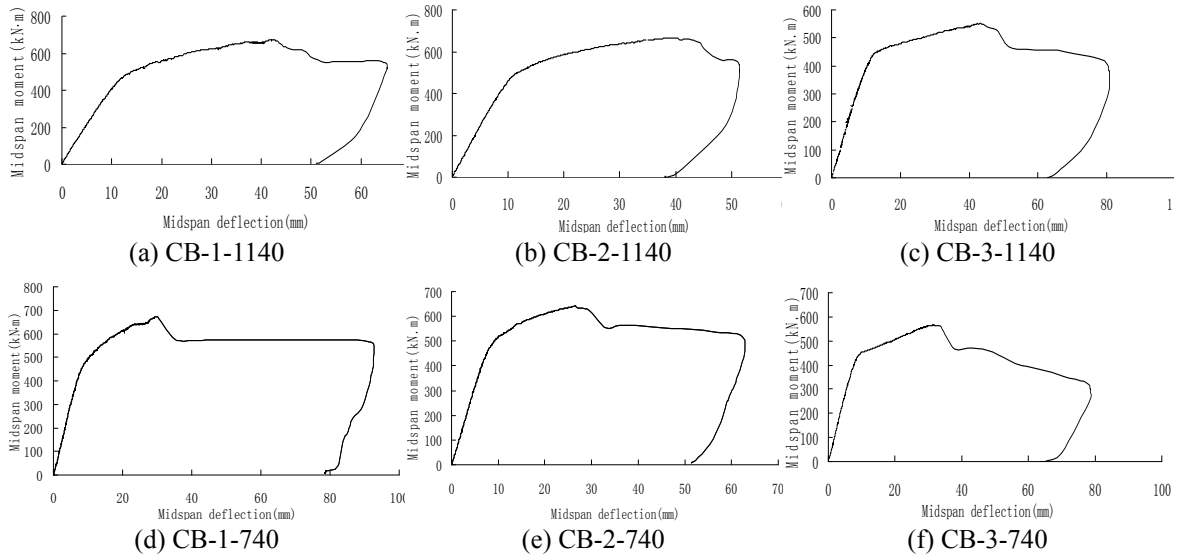

Fig. 11 Midspan moment-deflection curves of test beams

Table 3 Summary of the main test results

Specimen	L_0 (m)	λ	V_y (kN)	V_u (kN)	M_y (kN·m)	M_u (kN·m)	V_u / V_y	M_u / M_y
CB-1-1170	3100	3.1	394.4	591	394.4	673.7	1.71	1.71
CB-2-1170	3100	3.1	444.6	585	444.6	666.9	1.50	1.50
CB-3-1170	3100	3.1	426.4	483	426.3	550.6	1.29	1.29
CB-1-770	2300	2.0	481.0	909	481	672.7	1.40	1.40
CB-2-770	2300	2.0	472.9	870	472.8	643.8	1.36	1.36
CB-3-770	2300	2.0	416.6	766	416.6	566.8	1.36	1.36

Note: L_0 = the calculation span length; λ = shear span ratio, λ = a/h, a and h = shear span and height of the composite beam; V_y = yield shear strength; V_u = ultimate shear strength; M_y = yield moment strength; M_u = ultimate moment strength; δ_y = deflection that corresponds to the yield load; δ_u = deflection corresponding to the ultimate load

moment, which indicates that three types of beams have a proximal bending stiffness at elastic stage. The different inner steel forms have little influence on bending stiffness. The beam with steel form of type III has lower bending capacity than that of type II, but ductility ratio δ_u / δ_y is close. It is showed that corrugated steel web has little function to ductility improving. On the contrary, it brings down the carrying capacity. The beams with steel form of type I and type II have similar bending and shear strength, and ductility. It is showed that the top flange of steel has little utility in improving carrying capacity and ductility of the beam. It is a long process from yield moment to ultimate moment. The minimum moment ratio of ultimate and yield exceeded 1.29, which indicates that WESCC beams have not only high moment ratio of ultimate and yield but also good safety stock. Besides, ductility ratios of beams are all bigger than 3.22, which illuminates that WESCC beam has good ductility. Based on the above ductility, carrying capacity, safety stock and economy, the combination properties of the beam with inner steel form of type II is better than the others.

4. Bearing capacity calculation of WESCC beams

Some conclusions can been drawn from the experiment that: (1) The failure pattern of composite beams with shear span ratio of 2.0 is the concrete crushed at midspan. (2) PBL connectors can guarantee performance of joint work between steel girder and concrete. The specimens didn't damage for the failure of PBL connectors at the whole test procedure. (3) The carrying capacity of WESCC beam is evidently higher than that of traditional steel-concrete composite beam and reinforced concrete beam. It has large stiffness, safety margin and good ductility. Therefore, WESCC beam has good mechanical properties, construction technology and prospect of engineering application which can be used in bridge structures, large span structures, and high-level structure and so on. Based on experimental study and theoretical analysis, the calculation methods for the bearing capacity of bending and flexural rigidity have been proposed. The establishment and application conditions of bearing capacity formulas of WESCC beams are as follow.

4.1 Fundamental assumption

Based on the test results, the following basic assumptions are used to deduce calculation formulas of ultimate flexural capacity of WESCC beam. (1) Strain distribution of cross-section still conforms to plane cross-section assumption after the specimen deforming. (2) Tensile force in tensile region is undertaken by steel and reinforcement, and the role of concrete in tensile region is ignored. (3) The stress of steel and reinforcement are equal to product of strain and elastic modulus, which doesn't exceed design value. (4) Ultimate compressive strain ε_{cu} of concrete is 0.0033, compressive stress of concrete has been simplified as an equivalent rectangular.

4.2 The actual boundary of relatively height of compressive region

The yield sign of WESCC beam is that the bottom steel at the center of gravity reaches the yield strength f_{ya}, the boundary of relatively height of compressive region can be defined as the bottom tensile steel flange is yielding and the compressive strain of concrete is reaching the ultimate strain at the same time. As shown in Fig. 12, the actual boundary of relatively height ξ_b of compressive region can be calculated according to the following formulas.

$$\xi_b = \frac{x_c}{h_0} = \frac{1}{1+\dfrac{\varepsilon_{ya}}{\varepsilon_{cu}}} = \frac{1}{1+\beta_a} \tag{1}$$

$$\beta_a = \frac{\varepsilon_{ya}}{\varepsilon_{cu}} = \frac{f_{ya}}{E_a \varepsilon_{cu}} \tag{2}$$

where $h_0 = h - t / 2$; t = thickness of bottom steel; x_c = actual height of concrete in compressive region; E_a = modulus of steel; ε_{ya} = yield strain of steel; f_{ya} = yield strength of steel; β_a = ratio of steel yield strain and concrete ultimate compressive strain, it has influence on distinguishing of neutral axis and strain distribution of steel; In order to calculate the stress expediently at any depth of the cross-section of steel via plane cross-section assumption, x_c is used to calculate ξ_b. In order to ensure steel girder yield, the lower tensile steel flange yield, Eq. (3) should be satisfied.

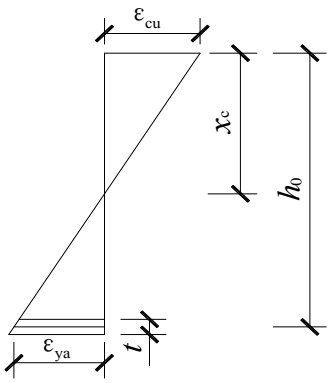

Fig. 12 Strain distribution of the limited failure

$$\xi \le \xi_b = \frac{1}{1+\beta_a} \tag{3}$$

4.3 Bearing capacity formula of WESCC beam

In order to make the calculation more convenient, some provisions are made to the symbols in Figs. 13-16. ch_0 is the distance between upper edge of lower hole on the web and the centroid of lower flange of girder. $\delta' h_0$ and wh_0 are respectively the distances from the centroid of top flange of steel girder to top of beam and to upper flange of lower hole on web , $\delta' + w + c = 1$. Three types of beam ignore the force function of steel web at the place from the centroid of top flange of girder to lower edge of upper hole on the web. As the distance between the second row reinforcement and neutral axis is relatively close, and it is better for calculating conveniently, applied force of the second row steel bars is ignored. According to different positions of neutral axis, calculation of bearing capacity of bending of WESCC beam can be divided into two cases. The first one case is the neutral axis gets across rib of beam. The second case is the neutral axis gets across top reinforced concrete flange plate of beam.

4.3.1 Bearing capacity calculation of the first case

When neutral axis gets across rib of beam, calculation can be divided into two types according to the condition whether the top flange of steel yields or not.

Type 1: The top compressive steel flange and lower tensile steel flange yield, the photo in Fig. 13 shows trapezoidal stress distribution of steel. The following formulas can be obtained form the equilibrium conditions.

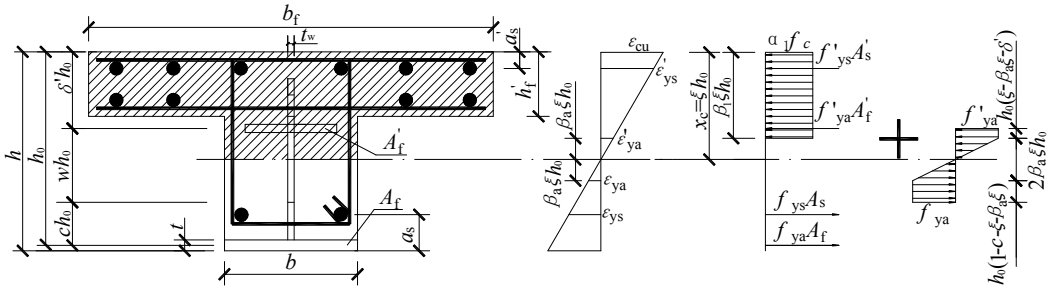

Fig. 13 Calculation diagram of type 1 of the first case

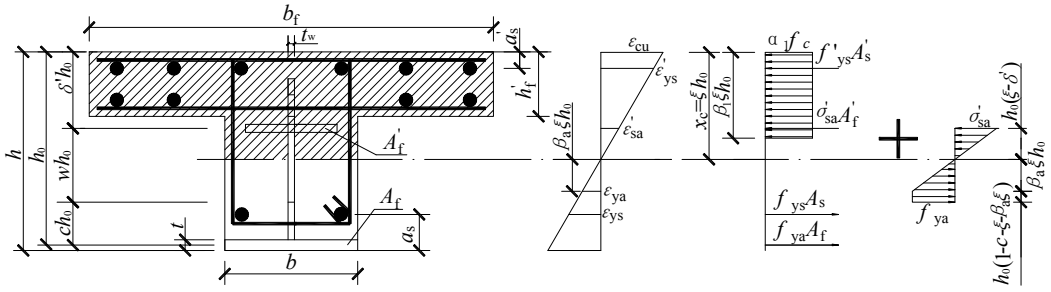

Fig. 14 Calculation diagram of type 2 of the first case

$$\alpha_1 f_c b\beta_1 \xi h_0 + \alpha_1 f_c h'_f (b'_f - b) + f'_{ys} A'_s + f'_{ya} A'_f + f'_{ya} h_0 t_w L_1 = f_{ys} A_s + f_{ya} A_f + f_{ya} t_w h_0 L_2 \quad (4)$$

$$\begin{aligned} M_u = {} & \alpha_1 f_c b\beta_1 \xi h_0 \left(h_0 - \frac{\beta_1 \xi h_0}{2} \right) + \alpha_1 f_c h'_f \left(b'_f - b \right) \left(h_0 - \frac{h'_f}{2} \right) + f'_s A'_s \left(h_0 - a'_s \right) \\ & + f'_{ya} A'_f \left(h_0 - \delta' h_0 \right) - f_{ys} A_s \left(a_s - \frac{t}{2} \right) + \frac{1}{3} f'_{ya} t_w \left(\beta_a \xi h_0 \right)^2 \\ & + f'_{ya} h_0 t_w L_1 \left(h_0 - \delta' h_0 - \frac{h_0}{2} L_1 \right) - f_{ya} t_w h_0 L_2 \left(c h_0 + \frac{1}{2} h_0 L_2 \right) \end{aligned} \quad (5)$$

where $L_1 = \xi - \beta_a \xi - \delta'$, $L_2 = 2 - c - \xi - \beta_a \xi$.

In order to ensure the lower steel flange yield, the formulas above should satisfy the Eq. (3).

In order to ensure the lower steel flange (or steel web at the centroid of the top steel flange) at the condition of compression and yield, the above formulas should satisfy the equation

$$\xi \geq \frac{\delta'}{1 - \beta'_a} \quad (6)$$

In order to ensure tensile steel bars of third row yield, the formulas above should satisfy the formula

$$\xi \leq \frac{(h - a_s)/h_0}{1 + \beta_s} \quad (7)$$

In order to ensure steel bars of the first row at the condition of compression and yield, the formulas above should satisfy the formula

$$\xi \geq \frac{a'_s / h_0}{1 - \beta'_s} \quad (8)$$

In the formulas above, if $A'_f \neq 0$, the above formulas can be applied to the beams with inner steel form of type I; if $A'_f = 0$, the above formulas can be applied to the beams with inner steel form of type II and III.

In basic formulas and applied conditions above, ξ is the actual boundary of relatively height of compressive region, α_1 is ratio of stress value of equivalent rectangular graph to axial compressive strength of concrete f_c, β_1 is coefficient of equivalent rectangular stress graph of concrete in compressive region, values of α_1 and β_1 are according to Code for Concrete Structure Design. A_f is area of top steel flange, A'_f is area of lower steel flange. t_w is thickness of steel web. a'_s is coverage thickness of steel bar in the top reinforced concrete flange plate, a_s is the distance from centroid of the third row steel bars to bottom steel plate. A_s is area of the first row steel bars, A'_s is area of the third row steel bars. f'_{ya} is tensile yield strength of steel, f_{ys} is tensile yield strength of steel bar. f'_{ys} is compressive yield strength of steel, f'_{ys} is compressive yield strength of steel bar. Strain ratio of steel to concrete is

$$\beta'_a = \frac{\varepsilon'_{ya}}{\varepsilon_{cu}} = \frac{f'_{ya}}{E_a \varepsilon_{cu}} \quad (9)$$

Type 2: The top compressive steel flange unyields and lower tensile steel flange yields, as shown in Fig. 14, stress distribution of steel are triangular and trapezoidal. The following formulas can be obtained from the equilibrium conditions

$$\begin{aligned}&\alpha_1 f_c b\beta_1\xi h_0+\alpha_1 f_c h_f'\left(b_f'-b\right)+f_{ys}'A_s'+\sigma_{sa}'A_f'+\frac{1}{2}\sigma_{sa}'t_w h_0\left(\xi-\delta'\right)\\&\quad=f_{ys}A_s+f_{ya}A_f+\frac{1}{2}f_{ya}t_w\beta_a\xi h_0+f_{ya}t_w h_0 L_1\end{aligned}\tag{10}$$

$$\begin{aligned}M_u=&\alpha_1 f_c b\beta_1\xi h_0\left(h_0-\frac{\beta_1\xi h_0}{2}\right)+\alpha_1 f_c h_f'\left(b_f'-b\right)\left(h_0-\frac{h_f'}{2}\right)\\&+f_s'A_s'\left(h_0-a_s'\right)+\sigma_{sa}'A_f'h_0\left(1-\delta'\right)-f_{ya}t_w h_0 L_2\left(ch_0+\frac{1}{2}h_0 L_2\right)\\&+\frac{1}{2}\sigma_{sa}'t_w h_0\left(\xi-\delta'\right)\left[h_0-\xi h_0+\frac{2}{3}h_0\left(\xi-\delta'\right)\right]\\&-f_{ys}A_s\left(a_s-\frac{t}{2}\right)-\frac{1}{2}f_{ya}t_w\beta_a\xi h_0\left[h_0-\xi h_0-\frac{2}{3}\beta_a\xi h_0\right]\end{aligned}\tag{11}$$

where $\sigma_{sa}'=f_{ya}\dfrac{\xi-\delta'}{\beta_a\xi}$, the expression of L_2 is the same as the former.

In order to ensure lower steel flange yield, the formulas above should satisfy the Eq. (3);

In order to ensure the third row tensile steel bars yield, the formulas above should satisfy the Eq. (7);

In order to ensure the compressive steel bars of first row yield, the formulas above should satisfy the Eq. (8);

If $\delta' \le \xi \le \delta' / (1-\beta'_a)$, the top steel flange (or steel web at the centroid of top steel flange) is in state of compression but not yielding. When equal sign of the equation $\delta' \le \xi \le \delta' / (1-\beta'_a)$ established, neutral axis gets across the centriod of the top steel flange and steel fibre at the centriod of lower steel flange reaches yielding state.

In order to ensure that top steel flange (or steel web at the centroid of top steel flange) is in state of compression but not yielding, the formulas above should satisfy the Eq. (12).

$$\delta'<\xi<\frac{\delta'}{1-\beta_a'}\tag{12}$$

The signs in above formulas and applied conditions are same as the formers.

4.3.2 The second calculation case of bearing capacity

If neutral axis gets cross top flange plate of reinforced concrete, calculation can be divided into two types according to the condition whether inner top steel flange yields or not.

Type 1: The top tensile flange and lower tensile steel flange yield, rectangle stress distribution of steel is shown in Fig. 15. The following formulas can be obtained from the equilibrium conditions.

$$\alpha_1 f_c b_f'\beta_1\xi h_0+f_{ys}'A_s'-f_{ya}'A_f'-f_{ys}A_s=f_{ya}A_f+f_{ya}t_w w h_0\tag{13}$$

$$M_u = \alpha_1 f_c b'_f \beta_1 \xi h_0 \left(h_0 - \frac{\beta_1 \xi h_0}{2} \right) + f'_s A'_s \left(h_0 - a'_s \right) - f'_{ya} A'_f \left(h_0 - \delta' h_0 \right) - f_{ys} A_s \left(a_s - \frac{t}{2} \right) - f_{ya} t_w w h_0 \left(c h_0 + \frac{w h_0}{2} \right) \tag{14}$$

In order to ensure tensile steel bars of the third row yield, the formulas above should satisfy the Eq. (7);

In order to ensure compressive steel bars of the first row yield, the formulas above should satisfy the Eq. (8);

In order to ensure the top steel flange (or steel web at the centroid of top steel flange) is in state of tensile and yielding, the formulas above should satisfy the equation

$$\xi \le \frac{\delta'}{1+\beta_a} \tag{15}$$

Synchronously, the formulas above has already satisfied the Eq. (3)

The signs in above formulas and applied conditions are the same as the former.

In the above formulas, if $A'_f \neq 0$, the formulas are applied to the calculation of composite beam with inner steel form of type I, or else, they are applied to the calculation of composite beam with inner steel form of type II and III.

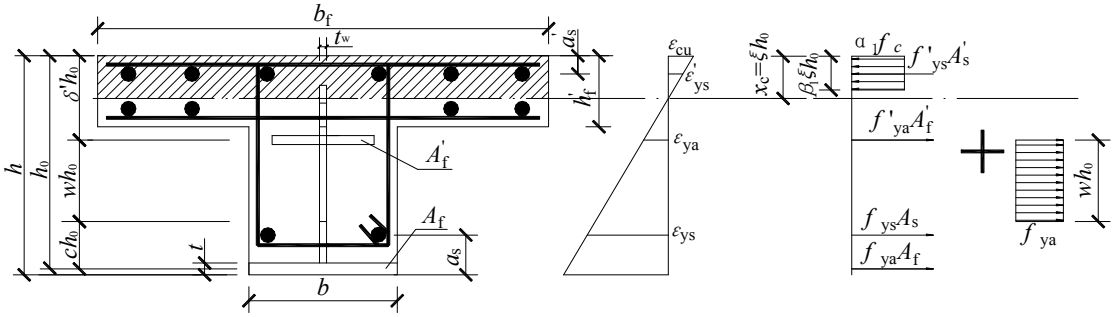

Fig. 15 Calculation diagram of type 1 of the second case

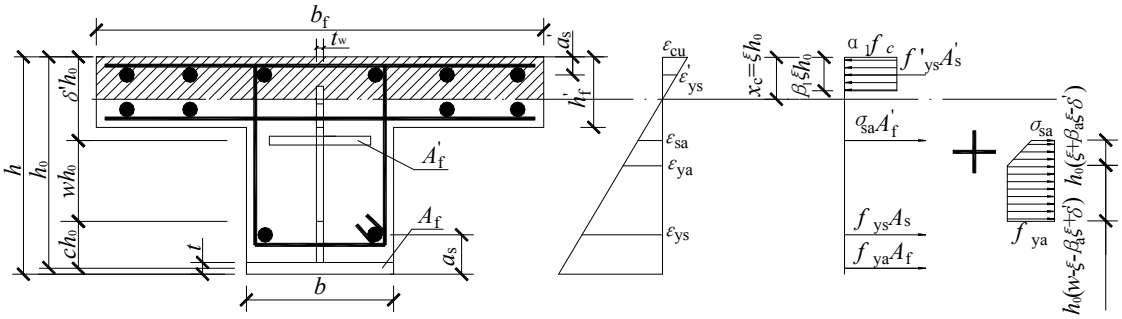

Fig. 16 Calculation diagram of type 2 of the second case

Type 2: The top tensile steel flange unyields, lower tensile steel flange yields, as shown in Fig. 16, graph of stress distribution of steel is trapezoidal. The following formulas can be obtained from the equilibrium conditions.

$$\alpha_1 f_c b'_f \beta_1 \xi h_0 + f'_{ys} A'_s - \sigma_{sa} A'_f - \frac{1}{2}\left(f_{ya} + \sigma_{sa}\right) t_w h_0 L_3 = f_{ys} A_s + f_{ya} A_f + f_{ya} t_w h_0 \left(w - L_3\right) \tag{16}$$

$$\begin{aligned} M_u = {} & \alpha_1 f_c b'_f \beta_1 \xi h_0 \left(h_0 - \frac{\beta_1 \xi h_0}{2} \right) + f'_s A'_s \left(h_0 - a'_s\right) - \sigma_{sa} A'_f h_0 \left(1 - \delta'\right) - f_{ys} A_s \left(a_s - \frac{t}{2} \right) \\ & + \frac{1}{2}\left(f_{ya} + \sigma_{sa}\right) t_w h_0 L_3 \left[h_0 \left(1 - \delta'\right) - \frac{2}{3} h_0 L_3 \right] + f_{ya} t_w h_0 \left(w - L_3\right) \left[c h_0 + \frac{1}{2} h_0 \left(w - L_3\right) \right] \end{aligned} \tag{17}$$

where $\sigma_{sa} = f_{ya} \dfrac{\delta' - \xi}{\xi \beta_a}$, $L_3 = \xi + \beta_a \xi - \delta'$

In order to ensure the lower steel flange yield, the formulas above should satisfy the Eq. (3);

In order to ensure tensile steel bars of the third row yield, the formulas above should satisfy the Eq. (7);

In order to ensure compressive steel bars of the first row yield, the above formulas should satisfy the Eq. (8);

If $\delta' \geq \xi \geq \delta' / (1 + \beta_a)$, the top steel flange (or steel web at the centroid of the top steel flange) is in tensile but did not reach yield condition. When equal sign of the equation $\delta' \geq \xi \geq \delta' / (1 + \beta_a)$ established, neutral axis gets cross the centriod of top steel flange and steel fibre at centriod of top steel flange reaches yielding state.

In order to ensure that top steel flange (or steel web at the centroid of top steel flange) is in state of tensile but not yielding, the formulas above should satisfy the formula

$$\delta' > \xi > \frac{\delta'}{1 + \beta_a} \tag{18}$$

The signs in above formulas and applied conditions are the same as the former.

In the formulas above, if $A'_f \neq 0$, the formulas are applied to the calculation of composite beam with inner steel form of type I, or else, they are applied to the calculation of composite beam with inner steel form of type II and III.

The calculation results of bearing capacity of bending according to the formulas deduced are shown in Table 4, some conclusions can be obtained from the calculation results. (1) As to the beam with inner steel form of type I and II, because of the discrete character of experiment, calculation results of bearing capacity of bending are in agreement with the test results except specimen CB-2-1140 which has a little warp between calculation results and test results. The average ratio of calculation value to test value is 0.989. (2) As to the beam with inner steel form of type III, there is a little warp between theoretical results of bearing capacity of bending and test results. The main reason is that the inner steel web in composite beam is corrugated. When specimen stays at elastic-plastic stage, deflection of beam becomes bigger and cracks develop sufficiently. The restraining action to steel web produced by concrete degenerates, which leads to a longitudinal deformation. A little folded effect of corrugated web led to decline in cross-section flexural capacity. Concrete and stirrup have a big restriction to corrugated web all the time, and hence the longitudinal deformation is just a little, which causes the theoretical results a little bigger

Table 4 Comparison between calculation and test results of bearing capacity

Specimens	L_0 (mm)	λ (mm)	M_u (kN·m)	M_{ut} (kN·m)	M_u/M_{ut}
CB-1-1140	3100	3.1	682.6	673.7	1.013
CB-1-740	2300	2.0	682.6	672.7	1.015
CB-2-1140	3100	3.1	630.4	666.9	0.945
CB-2-740	2300	2.0	633.5	643.8	0.984
Average value					0.989
CB-3-1140	3100	3.1	599.7	550.6	1.089
CB-3-740	2300	2.0	599.7	566.8	1.058
Average value					1.074

Note: L_0 is calculation span length; λ = shear span ratio, λ = a/h, a and h = shear span and height of the composite beam; M_u = the calculated ultimate moment strength; M_{ut} = recorded ultimate moment strength

than the test results. In actual project application of this type beam with corrugated web, the calculated result according to formulas deduced in the text should enlarge to 1.1 times, which takes into account the influence of longitudinal deformation imposes on bearing capacity of bending.

5. Calculation of flexural rigidity and deflection of composite beam

5.1 Calculation of flexural rigidity

Experimental results show that WESCC beams with shear span ratio of 3.1 and 2.1 damaged as typical bending failure mode, no slippage between the bottom steel plate and concrete was measured. The composite beams showed high composite function, the bottom steel plate and steel web can be utilized sufficiently. In order to deduce calculation methods of flexural rigidity of WESCC beams, approximate simplified method was used in the paper.(1) the lower steel flange

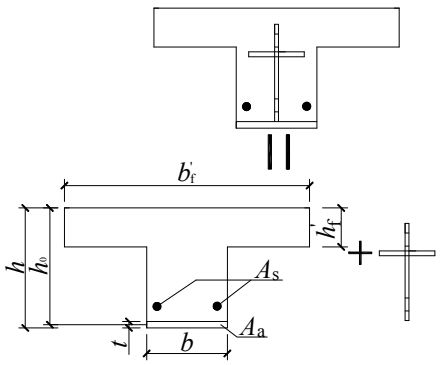

Fig. 17 Schematic of equivalent section of composite beams with steel form of type I

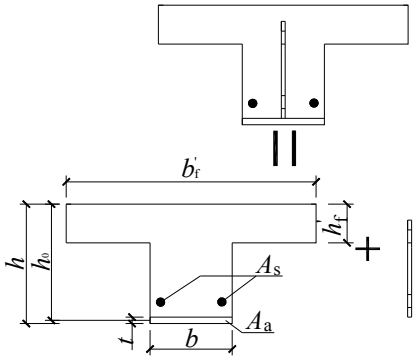

Fig. 18 Schematic of equivalent section of composite beams with steel form of type II, III

and concrete were equaled to T-shaped composite section; (2) Stiffness of composite beam is the stiffness summation of equivalent T-shaped composite section and the remaining part of steel section. (3) Flexural stiffness of equivalent T-shaped composite section calculated according to the calculation methods of flexural stiffness of reinforced concrete structures. As to composite beams with inner steel form of type I, II, III, calculation equivalent diagrams of section stiffness are shown in Figs. 17 and 18, stiffness of composite beam is equivalent to the above two parts, then the whole stiffness of composite beam is calculated by adding the two parts stiffness. The formulas of whole stiffness are as follow.

$$B_s = B_{rca} + B_a = \frac{E_a A_{sa} h_0^2}{1.15\psi + 0.2 + \dfrac{6\alpha_E \rho_{sa}}{1 + 3.5\gamma'_f}} + E_a I_a \tag{19}$$

where B_{rca} is section stiffness of lower steel flange and concrete;

B_a is stiffness of + -shaped and I -shaped steel sections.

E_a is elastic modulus of steel.

I_a is moment of inertia of + -shaped and – -shaped steel section.

$h_0 = h - t / 2$ is effective height of section.

$\Psi = 1.1 - 0.65 f_{tk} / (\rho_{te}\sigma_{sk})$ is non-uniformly distributed strain coefficient of bottom tensile steel plate.

$\rho_{te} = A_{sa} / A_{te}$ is sum of steel ratio and reinforcement ratio which calculated based on effective area of tensile concrete.

$\sigma_{sk} = M_{sk} / (0.87\ h_0 A_p)$ is profiled steel sheet stress which calculated based on the standard combination of load effect.

$A_{te} = bh / 2$ is section area of effective tensile concrete.

$\rho_{sa} = A_{sa} / (bh_0)$ is sum of reinforcement ratio and steel ratio of tensile steel and reinforcement in composite beam.

$\gamma'_f = (b'_f - b)\ h'_f / bh_0$ is area ratio of pressed flange and effective section area of web, if $h'_f > 0.2\ h_0$, then $h'_f = 0.2\ h_0$, the remaining symbols are the same as the formers.

Calculation results of the mid-span deflection which based on the calculation methods of flexural stiffness are shown in Table 5. Some conclusions can be got, calculation stiffness of

Table 5 Comparison between calculation and test results of midspan deflection

Specimen	40%P_u			50%P_u			60%P_u		
	f	δ	f/δ	f	δ	f/δ	f	δ	f/δ
CB-1-1140	4.45	6.4	0.70	5.65	8	0.71	6.75	9.9	0.68
CB-1-740	2.63	4.4	0.60	3.28	5.6	0.59	3.94	6.9	0.57
CB-2-1140	4.23	5.4	0.78	5.37	6.9	0.78	6.4	8.4	0.76
CB-2-740	2.33	4.1	0.57	2.95	5.1	0.58	3.55	6.2	0.57
CB-3-1140	3.55	5.3	0.67	4.5	6.6	0.68	5.45	8.2	0.66
CB-3-740	2.15	4.1	0.52	2.72	5.2	0.52	3.27	6.3	0.52
Average value			0.64			0.64			0.63

Note: f = calculated midspan deflection at elastic stage; δ = recorded midspan deflection at elastic stage

specimens is obviously larger and calculation deflection of specimens is significantly smaller, there is a big deviation between the theoretical value and experimental value. Further investigation needs to be done on WESCC beam.

5.2 Calculation of deflection (consideration of shear deflection)

Deflection of the beam in structural is composed of flexural deflection and shear deflection. As to the deflection of WESCC beam at normal use stage, we can get the elastic deflection formula of elastic body according to elastic displacement in structural mechanics

$$\Delta = \Delta_M + \Delta_J = \sum\int \frac{\overline{M}M_p}{EI}dx + \sum\int k\frac{\overline{F}_Q F_{QP}}{GA}dx \tag{20}$$

where Δ_M is bending deflection, Δ_J is shear deflection.

The shear deflection of beam is neglected in most cases, when ratio of length to height of beam less than 10, Wang (1985) pointed out that deflection caused by shear deflection shouldn't be neglected. The ratios of length to height of specimens in this paper are all less than 10, so the influence of shear deformation and cracks should be taken into account. When the deflection caused by shear is calculated, parameter $\beta(x)$ is introduced by (Yu 1960, Wang 1985) to concrete in composite beam which considering oblique cracks and non-flexible working of specimens. So the equation

$$\Delta_J = \sum\int k\frac{F_Q F_{QP}}{GA}dx \tag{21}$$

can be converted to the following equation.

$$\Delta_J = \sum\int k\frac{\overline{F}_Q F_{QP}}{GA}\beta(x)dx \tag{22}$$

where $\beta(x)$ =1, without oblique cracks and transverse cracks;

$\beta(x)$ = 4.8, the specimen has only oblique cracks but hasn't transverse cracks;

$\beta(x) = 3B / B_T$, the specimen has only transverse cracks or both transverse and oblique cracks, B is stiffness of specimen with cracks already formed, B_T is stiffness of specimen with cracks just formed.

$k = \frac{A}{I^2}\int_{A_1}\frac{S^2}{b^2}dA$, I is inertia of cross-section of composite beam, A is area of cross-section, S is static distance of part area A_1 of cross-section to the neutral axis, b is the lower width of section.

G_c is shear module of concrete, which is 0.4 times of concrete elastic module: $G_c = 0.4E_c$

A_1 is effective sheared area which is relative to calculated B_s (without taking the influence of tensile and cracked concrete into account), when calculating shear deflection, GA_j is used to replace GA;

As to composite beam of T-shaped section, when neutral axis passes through the top concrete flange of composite beam after cracking: $A_j = b'_f x$

When neutral axis passes through the rib of composite beam after cracking, $A_j = b'_f h'_f + b(x - h'_f)$, where, b'_f is width of top concrete flange, x is height of effective sheared concrete.

Table 6 shows the calculation results of stiffness which take the influence of shear deflection into account. Some conclusions can get from the calculation results: as to composite beam with ratio of length to height is less than 10, the calculation results which take shear deflection into account are in agreement with the test results, which the shear deflection shouldn't be neglected. The main reason is that composite beam of this type has much higher flexural capacity. The shear that specimens endured reached a quite high level when bending carrying capacity played to a certain extent. The shear stress and shear deformation also reached a certain level, which is especial and evident to composite beams with lesser ratio of length and height. Therefore, comparing to the traditional reinforced concrete beams and composite beams, it is necessary to consider the contribution of shear deflection on the basis of calculation of bending deflection when calculating the deflection of WESCC beams in this paper.

Table 6 Comparison between calculation and test results of midspan deflection (Consideration of shear deflection)

Specimen	40%P_u				50%P_u				60%P_u			
	Δ_J	Δ	δ_u	Δ/δ_u	Δ_J	Δ	δ_u	Δ/δ_u	Δ_J	Δ	δ_u	Δ/δ_u
CB-1-1140	1.65	6.1	6.4	0.95	2.05	7.70	8	0.96	2.476	9.226	9.9	0.93
CB-1-740	1.65	4.28	4.4	0.97	2.07	5.35	5.6	0.96	2.476	6.416	6.9	0.93
CB-2-1140	2.038	6.268	5.4	1.16	2.55	7.92	6.9	1.15	3.048	9.448	8.4	1.12
CB-2-740	1.846	4.176	4.1	1.02	2.3	5.25	5.1	1.03	2.769	6.319	6.2	1.02
CB-3-1140	1.67	5.22	5.3	0.98	2.08	6.58	6.6	1.00	2.5	7.95	8.2	0.97
CB-3-740	1.72	3.87	4.1	0.94	2.15	4.87	5.2	0.94	2.57	5.84	6.3	0.93
Average value				1.01				1.00				0.98
Overall average value						0.99						

Note: Δ_J = shear deflection; Δ = overall calculated deflection; δ_u = recorded deflection that corresponds to the ultimate load; P_u = ultimate load

6. Conclusions

This paper described a study on the behavior of WESCC beams which subjected to monotonic static loading. Six simply supported WESCC beams were tested with the shear span ratio and inner steel form as the main experimental parameters. The main conclusions drawn from this study are the following:

(1) The six WESCC beams suffered typical bending failure under monotonic static loading. The growth rate of cracks developed slowly during the whole test procedure and the integrity of specimens was good. Test phenomenon indicates that the concrete confined in the PBL and stirrups penetrated into the web of steel girder have effect on resisting longitudinal shear.
(2) The tested strain results indicate that longitudinal strain along the cross-section is near to linear distribution and the strain distribution of the section conforms to the plane cross-section assumption. Strain of bottom steel plate developed slowly when the specimens still stayed at elastic stage. But it developed fast when the specimens was at stage of elastic-plastic. The whole cross-section was almost plastic section while loading achieves to ultimate load. Steel of type II and type III in composite beams almost stayed in tensile region which were fully utilized.
(3) The WESCC beam went through the elastic stage, the elastic-plastic stage and the load degeneration stage during the whole test procedure.
(4) Three specimens with different inner steel form have proximal elastic bending stiffness and good ductility. Specimen with corrugated steel web has little function in ductility improving. In three types of beam with different inner steel forms, the behavior of beam with steel form of type II is best.
(5) Carrying capacity of bending and flexural rigidity of WESCC beams were theoretically analyzed.

As to the composite beams with inner steel form of type I and II, the calculation results of carrying capacity based on the formulas in this text are in agreement with test results. As to the composite beam with inner steel form of type III, the carrying capacity should take longitudinal deformation of corrugated steel web into account. The midspan deflection calculation results are in agreement with the test results, which bases on the calculation method of flexural rigidity that takes shear deflection into account. It demonstrates that the shear deflection should be taken into account. In general, the calculation methods of carrying capacity of bending, flexural rigidity and deflection suggested in this paper can be applied to design and calculation.

Acknowledgements

The authors would like to thank the financial support of the National Science Foundation of China (50708040) and “863” Technical Plan Project of China (2006AA11Z103). The authors also thank the assistance of the technicians at the Structure and Seismic Laboratory of Huaqiao University, China. All reviewers’ constructive comments and suggestions are gratefully appreciated.

References

Amadio C., Fedrigo C., Fragiacomo M. and Macorini, L. (2004), "Experimental evaluation of effective width in steel–concrete composite beams", *J. Constr. Steel Res.*, **60**(2), 199-220.

Benitez, M., Darwin, D. and Donahey, R. (1998), "Deflections of composite beams with web openings", *J. Struct. Eng.*, **124**(10), 1139-1147.

Cândido-Martins, J.P.S., Costa-Neves, L.F. and Vellasco, P.C.G. da S. (2010), "Experimental evaluation of the structural response of Perfobond shear connectors", *Eng. Struct.*, **32**(8), 1976-1985.

Johnson, R.P. (1982), *Composite Structure of Steel and Concrete*, Wiley-Blackwell Publishing.

Ju, Y.K., Kim, D.Y., Chung, K.R. and Kim, S.D (2001), "Composite action of the A-TEC beam with asymmetric steel section", *Archit. Inst. of Korea*, **17**(9), 49-56.

Ju, Y.K., Chun, S.C. and Kim, S.D. (2009), "Flexural test of a composite beam using asymmetric steel section with web openings", *J. Struct. Eng.*, **135**(4), 448-458.

Jurkiewiez, B. and Braymand, S. (2007), "Experimental study of a pre-cracked steel-concrete composite beam", *J. Constr. Steel Res.*, **63**(1), 135-144.

Lu, W.Y. (2006), "Shear strength prediction for steel reinforced concrete deep beams", *J. Constr. Steel Res.*, **62**(10), 933-942.

Medberry, S.B., Shahrooz, B.M. (2002), "Perfobond shear connector for composite construction", *AISC J.*, Chicago, **1**, 2-12.

Narayanan, R. (1988), *Steel-Concrete Composite Structures*, Spon Press Taylor and Francis Group.

Nie, J.G., Tang, L. and Cai, C. S.(2009), "Performance of steel-concrete composite beams under combined bending and torsion", *J. Struct. Eng.*, **135**(9), 1048-1057.

Nishiumi Kenji (1999), "Shear strength of perfobond rib shear connector under the confinement", *J. JSCE*, **633**, 193-203.

Oguejiofor, E.C. and Hosain, M.U. (1997), "Numerical analysis of push-out specimens with perfobond rib connectors", *Comput. Struct.*, **62**(4), 617-624.

Pecce, M., Rossi, F., Bibbò, F.A. and Ceroni, F. (2012), "Experimental behaviour of Composite Beams subjected to a hogging moment", *Steel and Composite Structures*, **12**(5), 395-412.

Valente, I.B. and Cruz, P.J.S. (2010), "Experimental analysis on steel and lightweight concrete composite beams", *Steel and Composite Structures*, **10**(2), 168-185.

Wang, C.Z. and Teng, Z.M. (1985), *The Theory of Reinforced Concrete Structure*, China Building Industry Press, Beijing, 350-351. [in Chinese]

Won, S.G., Bae, S.H., Jeong, W.B. and Bae, S.R. (2012), "Forced vibration analysis of damped beam structures with composite cross-section using Timoshenko beam element", *Structural Engineering and Mechanics*, **43**(1), 15-30.

Yu, W.W. and Winter G. (1960), "Instantaneous and long-time deflections of reinforced concrete beams under working loads", *ACI J.*, **57**(1), 29-50.

Zhang, N. and Fu, C.C. (2009), "Experimental and theoretical studies on composite steel–concrete box beams with external tendons", *Eng. Struct.*, **31**(2), 275-283.

CC